mm-Wave Joint Sensing and Communication System

Nima Souzandeh, Javad Pourahmadazar

Institut national
de la recherche
scientifique

Institut national
de la recherche
scientifique

mm-Wave Joint Sensing and Communication System

Nima Souzandeh[#1], Mehrdad Harifi-Mood[#], Javad Pourahmadazar[*], Sonia Aïssa[#] Serioja O. Tatu[#]

[#]Institut National de la Recherche Scientifique (INRS), Université du Québec, Canada

[*]Electrical and Computer Engineering, Concordia University, Canada

[1]nima.souzandeh@inrs.ca

***Abstract*— This work presents a new joint millimeter-wave sensing and communication system in the 24-GHz ISM band for detection, tracking, and vehicle-to-vehicle (V2V) communication. A calibrated tuning fork is used to test the effectiveness of the provided radar for a variety of frequencies. Then, a frequency-shift keying modulation scheme is proposed to enable this radar to work simultaneously as a sensing radar and communication transceiver. The proposed joint system's functionality for short-range applications with a data rate of 20 Kb/s is demonstrated by measurement results.**

***Keywords*— RF, mm-Wave, automotive radars, joint sensing and communication, V2V communication, FSK modulation.**

I. Introduction

Two of the most prevalent and significant uses of contemporary radio frequency (RF) technologies are radar and wireless communication. Target detection and identification are accomplished via radar, while information transfer between devices is accomplished using communication. They are often individually created and developed depending on the corresponding functions and frequency ranges.

Joint sensing and communication is a concept that has gained a lot of interest lately [1]. In terms of equipment cost and size, system performance, and spectrum consumption, joint systems are anticipated to offer substantial advantages. Both the system usage and system complexity should be significantly improved [2]. It is comprehensible in three different ways. First off, the communication subsystem adequately shares radar properties including high power, low side-lobe, strong directivity, and anti-interference. These benefits can strengthen information security, enhance communication quality, and broaden the reach of communication. Second, steady transmission has generally given radar many important benefits including minimal latency, easy installation, and quick response. Thirdly, the process of manual handling can be streamlined by increasing the automation level of dual-function devices. The applications of the intelligent transportation system (ITS) serve as one illustration of the benefits of this joint system.

Instead of relying on human judgment, the integrated approaches would enable next-generation vehicles to simultaneously reap the rewards of autonomously sensing the driving environment and cooperatively exchanging information with other vehicles about road conditions, speed, and any other vital information. [3].

Fig. 1 shows the future ITS applications scenario. As demonstrated, vehicles perceive their surroundings and communicate with one another as well as power beacons.

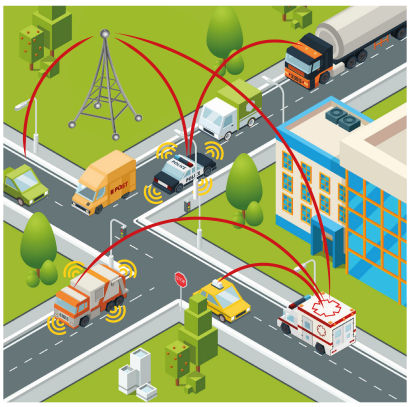

Fig. 1. The future ITS application scenario.

II. 24 GHz Continuous-Wave Doppler Radar

The description, block diagram, and characteristics of the deployed radar are presented in this section.

This is a transceiver sensor with in-phase and quadrature outputs, as seen in Fig. 2. The "Overview 24" commercial continuous-wave (CW) Doppler radar operates between 23.5 GHz and 24.5 GHz with a 1 GHz bandwidth (BW) deviation. [4]. It includes mainly two array antennas, a low noise microwave amplifier (LNA) with a gain of 20 dB, a controlled local oscillator, differential input mixers, baseband LNA, and a microwave amplifier (PA). It is a small embedded radar that can be integrated with many different kinds of equipment for a wide range of uses.

Generally, a Doppler CW radar sends out an unmodulated RF signal or energy to the target and waits for it to return. A portion of that signal reflects back to the radar. Therefore, the time it takes for this signal to return is a measure of the range to the target. Additionally, any movement on the target produces the Doppler effect and modulates the phase of the returned signal. In this way, the motion or velocity of the target is calculated.

Tuning forks are the targets in this experiment, which confirms the effectiveness of the radar detection system. We already know that tuning forks can generate exponentially-damped sinusoidal motions. As discussed in [5], with assuming the sinusoidal movement to be in the steady-state response of the fork movement. The baseband signal at the output of the sensor is expressed as a Bessel

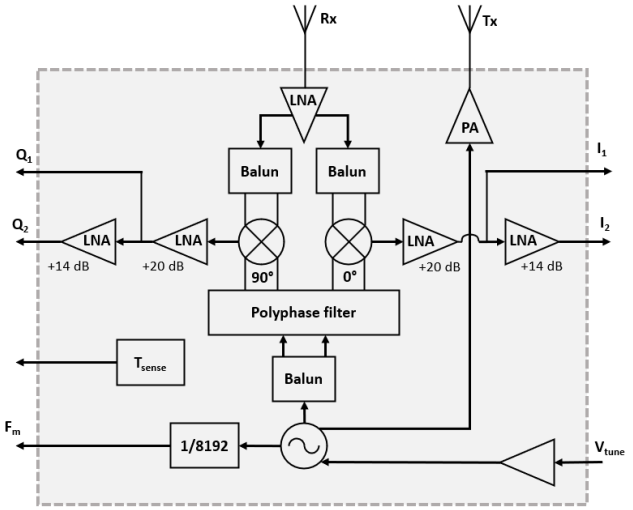

Fig. 2. The block diagram of the proposed 24 GHz radar.

function expansion of order n, $J_n(x)$. For a single tone target movement, $x(t) = m\sin(2\pi ft)$, the baseband output signal is expressed as:

$$B(t) = \sum_{n=-\infty}^{\infty} J_n\left(\frac{4\pi m}{\lambda}\right)\cos(2\pi nf)\cos\left(\frac{4\pi d}{\lambda}\right), \quad (1)$$

where, d the time-variant distance between the transceiver antennas and the target, can be written as $d(t) = d_0 + x(t)$. Here, $x(t)$ represents the movement of the tuning fork.

Equation (1) demonstrates that because of the non-linear nature of the cosine transfer function, harmonics will be created at the baseband output signal. The fork's vibrational amplitude and residual phase may be precisely calculated from the rate of the harmonics, and the movement frequency is acquired from the fundamental frequency of $B(t)$. The desired information regarding the movement of the target can be recovered by using the harmonics produced by the non-linear phase modulation. In Fig. 3 the fork is mounted on a pedestal as illustrated to stabilize it and prevent amplitude modulation brought on by hand motions. And the time domain I, and Q baseband signals are displayed on an Agilent DSO-X 2014A oscilloscope. Fig. 4 displays the measurement outcomes for several tuning forks.

The measurement findings show the expected frequency values for various tuning forks very clearly. According to

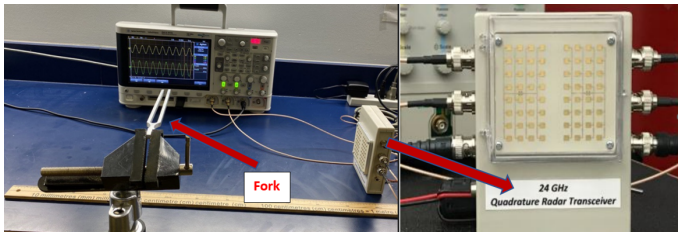

Fig. 3. The proposed radar setup for tuning fork measurement.

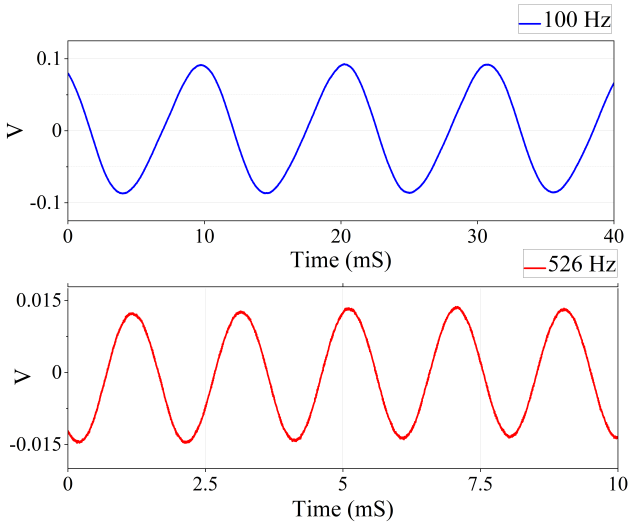

Fig. 4. Measurement results of 100 Hz and 528 Hz tuning forks

Fig. 4, the first harmonic's frequency is measured with a $\pm$ 2 Hz accuracy using the digital oscilloscope's measurement frequency tool to be the same as the mechanical oscillation frequency of the calibrated tuning fork.

III. Joint Sensing and Communications

As it is shown in the block diagram of the 24 GHz CW radar we can change the frequency of the transmitted signal with the V_{tune} voltage. Therefore, by connecting this V_{tune} to a multi-level waveform, we can transmit different frequencies, and use the radar as multiple frequency-shift keying (MFSK) modulator.

With the MFSK modulation technique, we are able to not only use this radar as a sensor but also communicate as a transceiver. It is noteworthy to say that in this work:

1) There is no need for any kind of synchronization between transmitter and receiver.
2) It is a very cost-effective system that has the lowest power consumption compared to other existing systems.

A. Operating Principle and Measurement Setup

This joint sensing and communication system is mainly supposed to be mounted on vehicles to make them work in two manners:

- Sensing the driving environment.
- Exchanging crucial information such as road or climate conditions, braking, and acceleration between vehicles or any other major information.

In our experiment, we use FSK modulation (M=2) and two identical quadrature radars as a transmitter (vehicle 1) and receiver (vehicle 2). The experiment setup and block diagram for better understanding are shown in Fig. 5 and 6 respectively.

A signal generator (1) that produces the pulse signal is connected to the V_{tune} of the transmitting radar (5). Quadrature I and Q signals are displayed and recorded by oscilloscopes

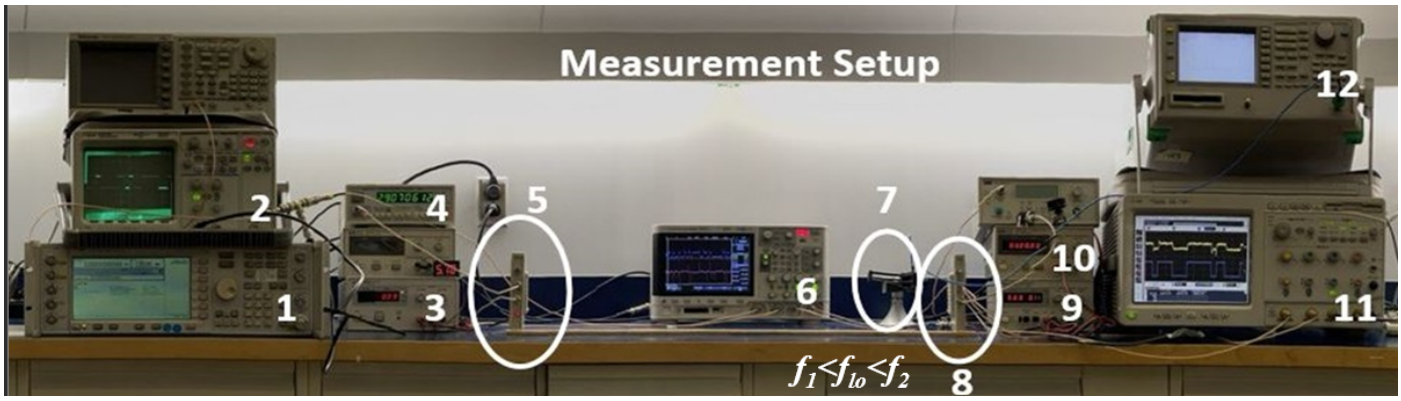

Fig. 5. Measurement setup

(2, 6, and 11), either in the transmitter or in the receiver. DC sources (3 and 9) are biasing the radars. The radar receiver (8) is tuned by a DC voltage (10). A frequency counter (4) is monitoring transmission at the 1/8192 output of the transceiver at port $\mathrm{F_m}$. Also, the local oscillator frequency of the receiver, (f_{LO}) should be located between the transmitted frequencies (f_1 and f_2) for demodulation. A Ka-band horn antenna (7) is connected to a spectrum analyzer (12) to monitor all the spectrum.

Fig. 7 shows the simplified block diagram of the demodulator in radar 2 (receiver). As it is seen, it includes a mixer, differentiator, and sample/hold blocks respectively.

In Fig. 7, we have;

$$S(t) = A \cdot \cos\left[2\pi f_{lo} \cdot t + \theta(t)\right] = \\ = \underbrace{A \cdot \cos\theta(t)}_{I(t)} \cdot \cos\left(2\pi f_{lo} \cdot t\right) - \underbrace{A \sin\theta(t)}_{Q(t)} \cdot \sin\left(2\pi f_{lo} \cdot t\right) \tag{2}$$

therefore I_1 and Q_1 are equal to:

$$\begin{cases} I_1(t) = \frac{A_1 \cdot A_2}{2}\left[\cos\left(2\pi f_{lo} \cdot t + \theta(t)\right) + \cos\theta(t)\right] \\ Q_1(t) = \frac{A_1 A_2}{2}\left[\sin\theta(t) - \sin(2\pi f_{lo} \cdot t + \theta(t))\right]. \end{cases} \tag{3}$$

Here, $\theta(t) = 2\pi k_f \cdot \int_0^t m(\tau)d\tau$, k_f = frequency sensitivity, and $m(r)$ = transmitted data (random pulse signal).

Therefore, I_3 and Q_3 are expressed as :

$$I_3(t) = \frac{d}{dt}\left[\frac{A}{2} \cdot \cos\left(2\pi k_f \cdot m(r) \cdot t\right)\right] = \\ \frac{A}{2} \cdot 2\pi k_f \cdot m(r)\left[-\sin\left(2\pi k_f \cdot m(r) \cdot t\right)\right] \tag{4}$$

$$Q_3(t) = \frac{d}{dt}\left[\frac{A}{2} \cdot \sin\left(2\pi k_f \cdot m(r) \cdot t\right)\right] = \\ \frac{A}{2} \cdot 2\pi k_f \cdot m(r)\left[\cos\left(2\pi k_f \cdot m(r) \cdot t\right)\right]. \tag{5}$$

There are two observations from equations (4) and (5).

First, if the data rate is sufficiently high there is not a significant discharge at the received pulse signal because of the S/H block. Second, if t is very short with help of this

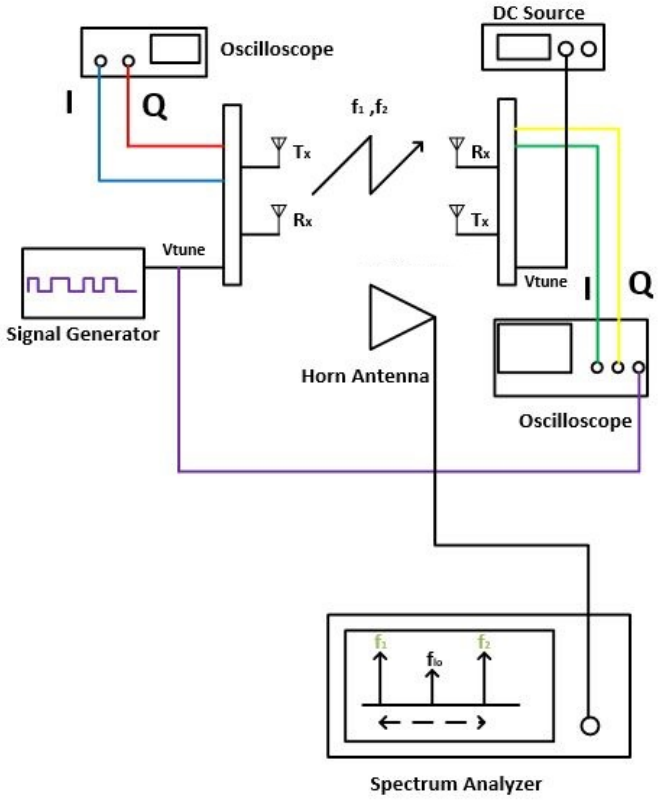

Fig. 6. Block diagram of the proposed joint system setup.

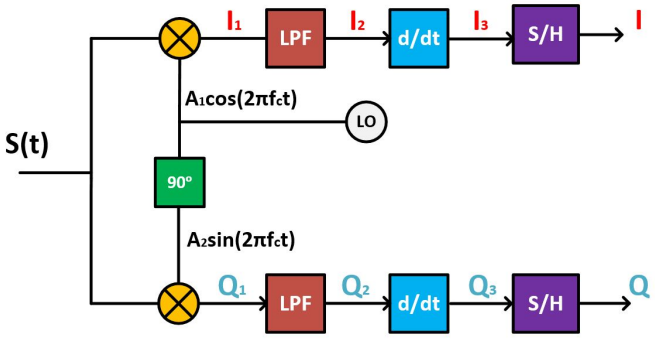

Fig. 7. Block diagram of the demodulator in radar 2.

estimation (if $x << 1, \sin x = x$ and $\cos x = 1$), we can simplify I_3 and Q_3 as below:

$$\begin{cases} I_3(t) \simeq -A \cdot \pi \cdot k_f \cdot m(r) \cdot 2\pi k_f \cdot m(r) \cdot t \\ Q_3(t) \simeq A \cdot \pi \cdot k_f \cdot m(r) \end{cases} \quad (6)$$

So, as it is shown the baseband I, Q signals after the S/H block if the data rate is high enough, will look like a pure pulse signal which follows the transmitted data signal. In the following, our measurement results will completely prove this phenomenon.

B. Measurement Results

Fig. 8 shows the transmitted random signal and received baseband in-phase signal at 20 Kb/s speed. As it is seen, the output fully follows the input signal. This proves equation (6). We move the transmission radar toward the reception radar with a constant speed of 2 Km/h to demonstrate the system's joint performance concurrently. As a result, as illustrated in Fig. 9, the target's movement causes us to get a sinusoidal signal at a frequency of 90 Hz (Doppler effect). But this signal also has the sent data stacked on top of it. In order to compare the pulse signal with the transmitted one more effectively, the sine wave's pulse signal is displayed closely in Fig. 10. As you can see, this comparison demonstrates the excellent bit error rate (BER) performance of our proposed joint system.

It is noteworthy to say that the data rate can be adjusted to easily distinguish it from Doppler in the baseband. For higher speeds, this will be increased in accord. As an example, for 100 Km/h relative speed a data rate of around 1 Mb/s is suggested.

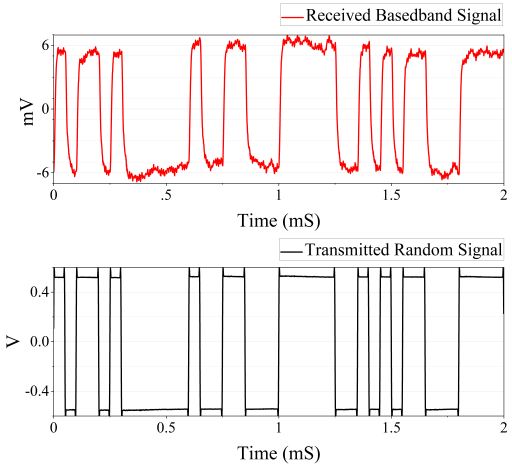

Fig. 8. Received baseband and transmitted random signal.

IV. Conclusion

Various scenarios using calibrated tuning forks are used to test radar experimentally for different frequencies as a human or vehicle detector and tracker. With an FSK modulation technique, two identical quadrature CW Doppler radars are used as a transmitter (vehicle 1) and receiver (vehicle 2)

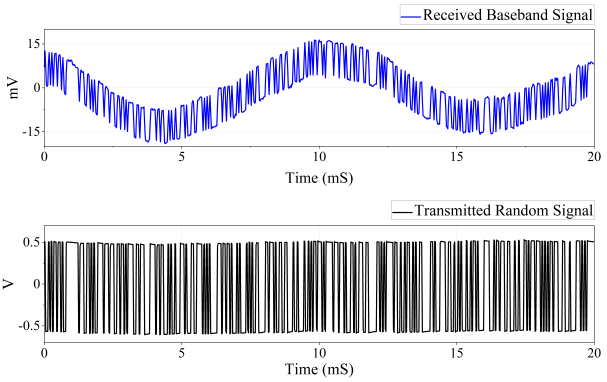

Fig. 9. Received baseband signal including Doppler effect and data on top and transmitted random signal.

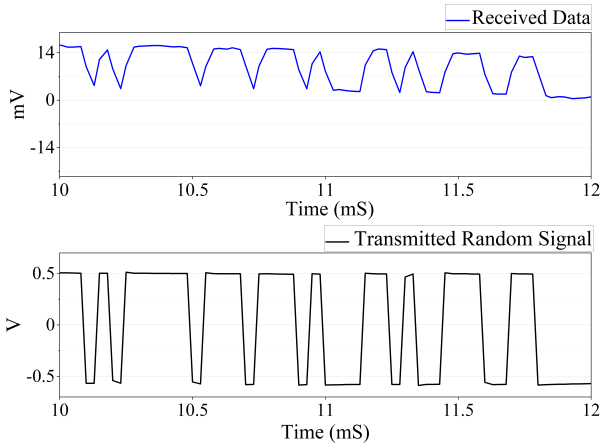

Fig. 10. Received and transmitted data.

for communicating crucial information. There are several key reasons that distinguish this work from the rest of the previous works that have been done in this field. First, sensing and communication are done simultaneously. Second, there is no need to synchronize the transmitter and receiver. And finally, it can be said that the design and construction of this system are very budget friendly with low power consumption.

References

[1] T. Wild, V. Braun, and H. Viswanathan, "Joint design of communication and sensing for beyond 5g and 6g systems," *IEEE Access*, vol. 9, pp. 30 845–30 857, 2021.

[2] B. Paul, A. R. Chiriyath, and D. W. Bliss, "Survey of RF communications and sensing convergence research," *IEEE Access*, vol. 5, pp. 252–270, 2016.

[3] J. Moghaddasi and K. Wu, "Multifunctional transceiver for future radar sensing and radio communicating data-fusion platform," *IEEE access*, vol. 4, pp. 818–838, 2016.

[4] H. Arab, S. Dufour, E. Moldovan, C. Akyel, and S. O. Tatu, "A 77-ghz six-port sensor for accurate near-field displacement and doppler measurements," *Sensors*, vol. 18, no. 8, p. 2565, 2018.

[5] Y.-B. Li, H.-L. Peng, M.-M. Li, W.-H. Li, C. Chen, and Q.-M. Wan, "A miniaturized and high frequency response 35ghz fmcw radar for short range target detections," in *2020 IEEE Electrical Design of Advanced Packaging and Systems (EDAPS)*. IEEE, 2020, pp. 1–3.